Controlling the B/Ti ratio of TiBx thin films grown by high-power impulse magnetron sputtering

Babak Bakhit, Ivan Petrov, Joseph E Greene, Lars Hultman, Johanna Rosén and Grzegorz Greczynski

Bakhit, B., Petrov, I., Greene, J. E, Hultman, L., Rosén, J., Greczynski, G., (2018), Controlling the B/Ti ratio of TiBx thin films grown by high-power impulse magnetron sputtering, *Journal of Vacuum Science & Technology. A. Vacuum, Surfaces, and Films*, 36(3), 030604.
https://doi.org/10.1116/1.5026445

Controlling the B/Ti ratio of TiB_x thin films grown by high-power impulse magnetron sputtering

Babak Bakhit,[a,*] Ivan Petrov,[a,b] J.E. Greene,[a,b] Lars Hultman,[a] Johanna Rosén,[a] and Grzegorz Greczynski[a]

[a] Thin Film Physics Division, Department of Physics (IFM), Linköping University, SE-58183 Linköping, Sweden

[b] Frederick Seitz Materials Research Laboratory and Department Materials Science, University of Illinois, Urbana, Illinois 61801, USA

Abstract

TiB_x thin films grown from compound TiB_2 targets by magnetron sputter deposition are typically highly over-stoichiometric, with x ranging from 3.5 to 2.4, due to differences in Ti and B preferential-ejection angles and gas-phase scattering during transport from the target to the substrate. Here, the authors demonstrate that stoichiometric TiB_2 films can be obtained using high-power impulse magnetron sputtering (HiPIMS) operated in power-controlled mode. The B/Ti ratio x of films sputter-deposited in Ar is controllably varied from 2.08 to 1.83 by adjusting the length of HiPIMS pulses t_{on} between 100 and 30 μs, while maintaining average power and pulse frequency constant. This results in peak current densities $J_{T,peak}$ ranging from 0.27 to 0.88 A/cm^2. Energy- and time-resolved mass spectrometry analyses of ion fluxes incident at the substrate position show that the density of metal ions increases with decreasing t_{on} due to a dramatic increase in $J_{T,peak}$ resulting in strong gas rarefaction. With t_{on} < 60 μs ($J_{T,peak}$ > 0.4 A/cm^2), film growth is increasingly controlled by ions incident at the substrate, rather than neutrals, as a result of the higher plasma dencity and, hence, electron-impact ionization probablity. Thus, since sputter-ejected Ti atoms have a higher probability of being ionized than B atoms, due to their lower first-ionization potential and larger ionization cross-section, the Ti concentration in as-deposited films increases with decreasing

* Corresponding author.
Email address: babak.bakhit@liu.se (B. Bakhit)

t_{on} (increasing $J_{T,peak}$) as ionized sputtered species are steered to the substrate by the plasma in order to maintain charge neutrality.

1. Introduction

TiB_2, which has a hexagonal AlB_2 crystal structure,[1] is a hard (reported hardness values range from 30 to 60 GPa),[2-4] high-melting-point (3226 °C),[5] refractory ceramic with excellent tribological[6-8] and corrosion-resistance[9,10] properties, relatively low electrical resistivity (reported values range from 6.6 to 400 μΩ.cm),[11-14] and high thermal and chemical stability.[14] TiB_2 thin films are used to increase the wear life and abrasion resistance of cutting tools,[7] dies,[15] and engine components.[16] However, a common issue in sputter-deposited TiB_x is that the films contain excess B with x ranging from 3.5 to 2.4.[16-19] While excess B can lead to the formation of interesting nanostructures with enhanced hardness,[17,20,21] it is important to be able to control the B/Ti ratio, and hence film properties, during deposition.

The underlying mechanisms leading to the incorporation of excess B in magnetron sputter-deposited TiB_x films were established by Neidhardt et al.[22] who showed that, due to differences in mass mismatch between Ar^+ sputtering-gas ions (m_{Ar} = 39.9 amu) and the target constituents B and Ti (m_B = 10.8 and m_{Ti} = 47.9 amu), sputtered B atoms are preferentially ejected along the target normal, while the Ti angular ejection distribution is under-cosine, extending toward lower angles. As a result, films deposited on substrates facing a TiB_x target contain excess B. Increasing the sputtering pressure, and/or the target-to-substrate distance, reduces the Ti deficiency due to the higher gas-phase scattering probability of light B atoms during transport to the substrate.[22] An increase in the substrate bias also leads to a limited decrease in the B/Ti ratio as a result of preferential B resputtering.[2] One approach for obtaining stoichiometric TiB_2 films was recently demonstrated by Petrov et al.,[23] who used highly-magnetically-unbalanced magnetron

sputtering to selectively ionize sputter-ejected Ti atoms which are steered via a tunable external magnetic field to the growing film; the B/Ti ratio was thus controlled by varying the field strength of the external Helmholtz coils.

High-power impulse magnetron sputtering (HiPIMS)[24,25] has also been used to grow TiB_x films.[17] In HiPIMS, relatively high power is applied to the target in short pulses in order to increase the plasma density and, thus, the ionization efficiency of sputter-ejected atoms. At constant average power, the HiPIMS pulse length and frequency are the primary parameters that influence the peak target current density which, in turn, determines the degree of plasma ionization.[24-26] Nedfors et al. found that varying the HiPIMS pulse frequency between 200 and 1000 Hz (corresponding to $J_{T,peak}$ values of 1.18 to 0.11 A/cm^2) with a relatively long pulse length of 200 μs and a constant target power, resulted in only a minor change in the B/Ti ratio of films sputter deposited from a TiB_2 target in Ar.[17]

In the experiments described below, we take a different approach and investigate the effect of decreasing HiPIMS pulse lengths t_{on} from 100 to 30 μs at constant frequency and target power to demonstrate that this provides a straightforward approach for controlling the B/Ti ratio in as-deposited layers. We find that as t_{on} is decreased below ~60 μs, the peak discharge current $J_{T,peak}$ increases sufficiently that, due to strong Ar gas rarefaction, the plasma becomes dominated by metal ions as shown by *in-situ* mass spectrometry. The lower first-ionization potential and higher electron-impact ionization cross-section of Ti vs. B, and hence higher Ti^+ than B^+ flux, provides the ability to controllably and continuously decrease the film B/Ti ratio, from 2.08 with t_{on} = 100 μs to 1.83 with t_{on} = 30 μs, due to plasma steering of the ions to the growth surface.

2. Experimental procedure

TiB_x layers, 1-μm thick, are grown in a CC800/9 CemeCon AG system by sputtering, in HiPIMS power-controlled mode, from a TiB_2 target in Ar (99.999% pure) discharges at a constant power of 3 kW with a 1 kHz pulse frequency. The duty cycle ranges from 10% with t_{on} = 100 μs to 3% with t_{on} = 30 μs. CemeCon AG provided the 8.8×50 cm^2 TiB_2 target (purity > 98%). The sputtering system, described in detail elsewhere,[27] has a base pressure of 6×10^{-6} Torr (0.8×10^{-3} Pa).

Si(001) substrates, 1.5×1.5 cm^2, are cleaned in sequential ultrasonic acetone and isopropanol baths and then mounted on a substrate holder with clips, to ensure good electrical contact, and loaded into the sputtering chamber facing the center of the target with a target-to-substrate separation of 18 cm. During film growth, substrates are electrically floating with a negative potential V_s, which is a function of the HiPIMS pulse width and varies during each pulse between 15 V and $V_{s,max}$, in which $V_{s,max}$ increases continuously from 25 V for 100-μs pulses to 35 V for 30-μs pulses. Film deposition is carried out at 450 °C in Ar at a pressure of 3 mTorr (0.4 Pa) after sputter-cleaning the target behind a closed shutter at 2 kW for 30 s. TiB_x film thicknesses are determined from cross-sectional images, acquired using a Zeiss LEO 1550 scanning electron microscope (SEM), of cleaved samples.

TiB_x film compositions are obtained using a Kratos Axis Ultra DLD x-ray photoelectron spectroscopy (XPS) system with monochromatic Al-K_α radiation ($h\nu$ = 1486.6 eV). In order to remove surface contamination prior to analyses, samples are sputter-etched for 120 s using 4 keV Ar^+ ions, incident at 70° with respect to the sample normal, followed by 600 s with 0.5 keV Ar^+ to minimize the influence of sputter artefacts on the extracted B/Ti ratios.[28] The XPS sensitivity factors are calibrated using the results of time-of-flight elastic recoil detection analyses (ToF-ERDA) of selected TiB_x samples. The ToF-ERDA measurements were carried out using a tandem accelerator with a 36 MeV $^{127}I^{8+}$ probe beam incident at 67.5° with respect to the sample surface normal; recoils are detected at 45°.

A Hiden Analytical EQP1000 instrument is utilized to perform *in-situ* time-dependent mass- and energy-spectroscopy analyses of ion fluxes incident at the substrate position during HiPIMS sputtering of the TiB_2 target under the same conditions as during film deposition. The orifice of the spectrometer is placed at the substrate plane, facing the center of the target. Ion-energy distribution functions (IEDFs) are recorded during 100 consecutive HiPIMS pulses such that the total acquisition time per data point is 1 ms. The ion energy is scanned between 1 and 50 eV in 0.5 eV steps. Additional details regarding the IEDF measurements, including mass-dependent ion time-of-flight corrections, are given in Refs. [29, 30]. A Tektronix 500 MHz digital oscilloscope is used to measure target current and voltage waveforms.

3. Results and discussion

Fig. 1 shows target voltage $V_T(t)$ and current density $J_T(t)$ waveforms as a function of t_{on} during HiPIMS sputtering of TiB_2. The observed oscillations in $V_T(t)$, and the corresponding low-amplitude current transients in $J_T(t)$, which occur after terminating the pulses, are attributed to the RLC circuit formed between the electronic switch of the HiPIMS power supply, connecting cable, and the target. At t_{off}, the capacitor bank is discounected; however, the energy of the magnetic field flux induced by the current $J_T(t_{off})$ still has to be dissipated, thus generating RLC-type oscillations.[31] The negative target ignition voltage $V_T(t=0)$, ~600 V, is independent of t_{on}, and $V_T(t)$ decreases with time to reach 395, 400, 418, 435, 460, and 500 V for pulse lengths of 100, 80, 60, 50, 40, and 30 µs, respectively, due to the capacitor bank size. The shape of the $J_T(t)$ waveforms changes from being relatively flat with a slow rise time and an abrupt decrease with $t_{on} \leq 60$ µs to a more gradual decay with t_{on} = 80 and 100 µs. However, the most pronounced effect of decreasing the pulse length from 100 to 30 µs is a dramatic increase in the peak current density $J_{T,peak}$ from 0.27 to 0.88 A/cm^2

as shown in the inset of Fig. 1. At shorter pulse lengths, J_T decreases rapidly (within a few μs) once $J_{T,peak}$ is reached.

Ti^+, Ti^{2+}, Ar^+, and B^+ ion intensities F incident at the substrate plane are plotted as a function of the HiPIMS pulse length t_{on} in Fig. 2(a). Ar^{2+} and B^{2+} ion intensities are both < 0.5% of the total intensity due to the high second-ionization potential of Ar, IP_2^{Ar} = 25.6 eV,[32] and the fact that the second-ionization potential of B, IP_2^B = 25.2 eV,[32] is much greater than the first-ionization potential of Ar, IP_1^{Ar} = 15.8 eV.[32] Thus, Ar^{2+} and B^{2+} ion intensities are not shown in Fig. 2(a). For $t_{on} \geq 80$ μs, the incident ion intensity is dominated by gas ions, with $F_{Ar^+} > 50\%$. However, as the peak current density $J_{T,peak}$ increases with $t_{on} < 60$ μs, F_{Ar^+} decreases below 10% and the Ti^+ ion flux becomes dominant with $F_{Ti^+} > 60\%$, due to Ar rarefaction and quenching of electron-energy distribution. The B^+ and Ti^{2+} ion intensities also increase with decreasing t_{on}; however, the B ionization rate remains, over the entire t_{on} range, much lower than that of Ti because of the combination of a higher first-ionization potential (IP_1^B = 8.3 eV vs. IP_1^{Ti} = 6.8 eV)[32] and a smaller electron-impact ionization cross-section,[33] as shown in Table 1. Even though the composition of the steady-state sputtered-atom flux is the same as that of the bulk target (B/Ti = 2),[34] the measured B^+/Ti^+ ion-intensity ratio at the substrate plane ranges from ~0.1 with 100 μs to 0.4 at 30 μs.

The observed drop in F_{Ar^+} as a function of decreasing pulse length t_{on} in Figure 2(a) is a consequence of the transition from an Ar-gas-dominated discharge to a metal-vapor-dominated discharge as a result of strong gas rarefaction, which increases with increasing $J_{T,peak}$.[25,35-40] In addition to a reduced Ar gas density in the intense plasma region, the Ar ionization probability is also suppressed as a result of quenching the electron-energy distribution in the Ti^+-dominated plasma since IP_1^{Ti} is much lower, by more than 50%, than IP_1^{Ar}.

TiB_x film-growth rates R vs. t_{on} are plotted in Fig. 2(b). R decreases from 11.4 Å/s with t_{on} = 100 μs to 8.0 Å/s with t_{on} = 30 μs due primarily to the back-attraction of metal ions to the target,[41-43] which becomes more pronounced as the plasma transitions from Ar^+-ion controlled to metal-ion controlled. That is, an increasing fraction of sputtered atoms no longer contributes to film growth as t_{on} is decreased. Fig. 2(c) shows that the B/Ti ratio of as-deposited TiB_x layers, which is 2.08 for t_{on} = 80 and 100 μs, decreases rapidly at lower pulse lengths to 1.83 at t_{on} = 30 μs.

A confirmation of the significant role of gas rarefaction in controlling TiB_x film composition is provided in Fig. 3, which shows typical B^+ and Ti^+ IEDFs during, and after, HiPIMS pulses with lengths t_{on} = 40 and 80 μs. The Ti^+ IEDFs for 40-μs pulses (Fig. 3(a)) exhibit broad peaks with high-energy tails, which we attribute to a superposition of Sigmund-Thompson sputtered-species energy distributions[44,45] and ion acceleration by the combination of plasma and floating potentials with HiPIMS plasma instabilities due to plasma collective effects.[46,47] The broad Ti^+ ion energy distributions, first observed in the IEDF acquired at t = 32 μs after igniting the pulse (there is no significant Ti^+ energy tail at shorter times), are essentially preserved throughout the entire remaining time period investigated, up to 152 μs. Thermalization of Ti^+ ions due to collisions with Ar atoms between the target and the substrate plane is negligible, as evidenced by the small intensity of the low-energy peak centered at ~2.5 eV and assigned to thermalized ions.[48]

B^+ IEDFs for t_{on} = 40 μs pulses (Fig. 3(b)) exhibit broad IEDFs throughout the entire time period analyzed. The earlier appearance of B^+ ions, present in IEDFs acquired at t = 23 μs after ignition, is a consequence of their higher velocity resulting primarily from having a lower mass (m_B/m_{Ti} = 0.23). The high velocity gives rise to even fewer gas phase collisions; hence, there is no low-energy thermal B^+ peak.

In contrast to IEDF results with 40-μs-long HiPIMS pulses, Ti^+ IEDFs with t_{on} = 80 μs (Fig. 3(c)) contain high-energy components only for t ≤ 90 μs. At longer times, a low-energy thermalized peak appears near 2.5 eV, and eventually dominates IEDFs obtained at t > 130 μs. The strong Ti^+ thermalization observed in the longer HiPIMS pulses stems from a reduction in Ar gas rarefaction due to lower target current densities (Fig. 1) together with a slow decay in J_T which allows Ar refill in the near-target region. The latter effect has also been recently demonstrated for HiPIMS sputtering of a Ti target in pure Ar.[49,50] B^+ IEDFs with t_{on} = 80 μs (Fig. 3(d)), however, do not contain thermalized peaks, even at times out to t = 152 μs. While the Ti to Ar mass ratio is near unity (m_{Ti}/m_{Ar} = 1.20), resulting in efficient energy and momentum transfer during collisions, the B to Ar mass ratio is only 0.27; hence, there is very little thermalization.

Shortening the pulse length at constant total power and pulse frequency during HiPIMS sputtering of TiB_2 in Ar at 3 mTorr gives rise to a monotonic decrease in the B/Ti ratios of as-deposited TiB_2 films from 2.08 to 1.83; i.e., the film composition can be tuned across the stoichiometric value. The ability to controllably vary the film composition is due to changes in the gas-phase transport of sputter-ejected B and Ti atoms as a result of the transformation from inert-gas-dominated discharges to metal-ion-dominated discharges which occurs as t_{on} is decreased below ~60 μs. This transition is caused by gas rarefaction due to momentum transfer to the Ar gas from the high flux density of sputtered species[51] ("the sputtering wind").[52]

With t_{on} > 60 μs, the peak current density is < 0.3 A/cm^2 and the J_T pulse shape is relatively flat over much of the pulse, while tapering off toward the end. Mass spectrometry results show that the ion flux incident at the substrate position is dominated by Ar^+. At these pulse lengths, the system is essentially operating in a manner similar to pulsed dc magnetron sputtering mode.[53-55] As t_{on} is decreased below 60 μs, the peak current densities exceed 0.4

A/cm^2, and mass spectrometry results show that the discharge is metal-ion dominated with the target current density truncated at the end of the pulse, thus eliminating current tapering and, hence, minimizing Ar refill effects,[31] which tend to move the discharge toward being Ar-gas-dominated. Sputter-ejected Ti atoms have a lower ionization potential and a larger electron-impact ionization cross-section than B, and thus have a higher ionization probability in the discharge. Indeed, the measured B^+ intensity at the shortest pulse, t_{on} = 30 μs, is ~40% smaller than the Ti^+ intensity despite the fact that the sputter-ejected B/Ti ratio is two. Since ionized species are directed to the substrate by the plasma plume, the *total* Ti flux (ions plus neutrals) to the substrate increases relative to that of B as Ti ions are guided to the growing film.

The IEDFs in Figure 3 show that for shorter pulses, the average ion energy increases, with high-energy tails extending out to > 150 μs. In order to assess whether preferential B resputtering from the growing film has a significant role in reducing the B/Ti ratio as t_{on} is decreased, TiB_x films were grown with t_{on} values of 50 and 100 μs as a function of negative substrate bias amplitude, varied between 50 and 100 V, applied in synchronous with the HiPIMS pulses. Film compositions were found to be identical, within measurement uncertainty, to layers grown at floating potential. Thus, we conclude that resputtering does not play a major role in controlling the TiB_x film composition in our experiments.

4. Conclusions

In summary, we have demonstrated that the composition of TiB_x films grown by HiPIMS sputtering from a TiB_2 target in Ar can be continuously and controllably varied from over-stoichiometric to stoichiometric to under-stoichiometric by decreasing the HiPIMS pulse length t_{on}, while all other parameters are maintained constant. Time-dependent IEDFs confirm the influence of the pulse length on the degree of gas rarefaction. With t_{on} < 60 μs,

the IEDFs are preserved long after the pulse, whereas the IEDFs collapse into a thermalized low-energy peak for longer pulses. Film growth with $t_{on} < 60$ μs is increasingly controlled by incident ions rather than neutrals. Thus, since sputter-ejected Ti atoms have a higher probability of being ionized in the plasma than B atoms, due to their lower first-ionization potential and larger ionization cross-section, the Ti concentration in as-deposited films increases with decreasing t_{on} as ionized sputtered species are steered to the substrate by the plasma in order to maintain charge neutrality.

Acknowledgements

The authors gratefully acknowledge Jens Jensen for assistance with ToF-ERDA analyses and Todor Donchev for useful discussions. Financial support from the Swedish Research Council VR Grant 2014-5790 and 642-2013-8020, the Knut and Alice Wallenberg foundation for a Fellowship Grant and Project funding (KAW 2015.0043), an Åforsk foundation grant #16-359, and Carl Tryggers Stiftelse contracts CTS 15:219, CTS 17:166, and CTS 14:431 is gratefully acknowledged. We thank CemeCon AG for providing the TiB_2 target for these experiments. The authors also appreciate the financial support of the Swedish Government Strategic Research Area in Materials Science on Functional Materials at Linköping University (Faculty Grant SFO Mat LiU No. 2009 00971).

References

1. P. Vajeeston, P. Ravindran, C. Ravi, and R. Asokamani, Phys. Rev. B 63, 045115 (2001).
2. M. Berger, M. Larsson, and S. Hogmark, Surf. Coat. Technol. 124, 253 (2000).
3. F. Lofaj, T. Moskalewicz, G. Cempura, M. Mikula, J. Dusza, and A. Czyrska-Filemonowicz, J. Eur. Ceram. Soc. 33, 2347 (2013).

4. M. Mikula, B. Grančič, T. Roch, T. Plecenik, I. Vávra, E. Dobročka, A. Šatka, V. Buršíková, M. Držík, M. Zahoran, A, Plecenik, and P. Kúš, Vacuum 85, 866 (2011).
5. H. Holleck, J. Vac. Sci. Technol. 6, 2661 (1986).
6. M. Berger, L. Karlsson, M. Larsson, and S. Hogmark, Thin Solid Films 401, 179 (2001).
7. "Handbook of Chemistry and Physics", 85th ed., edited by D. R. Lide (CRC, Boca Raton, FL, 2004).
8. C. Mitterer, J. Solid State Chem. 133, 279 (1997).
9. A.S. Dranenko, V.A. Lavrenko, and V.N. Talash, Powder Metall. Met. Ceram. 49, 174 (2010).
10. I.I. Korobov, G.V. Kalinnikov, A.V. Ivanov, N.N. Dremova, R.A. Andrievski, and S.P. Shilkin, Prot. Met. Phys. Chem. Surf. 52, 618 (2016).
11. A.D. McLeod, J.S. Haggetry, and D.R. Sadoway, J. Am. Ceram. Soc. 67, 705 (1984).
12. A. Shutou, T. Matsui, H. Tsuda, H. Mabuchi, and K. Morii, Mater. Lett. 45, 143 (2000).
13. V. Ferrando, D. Marre, P. Manfrinetti, I. Pallecchi, C. Tarantini, and C. Ferdeghini, Thin Solid Films 444, 91 (2003).
14. M.V. Frandsen, and W.S. Williams, J. Hard Mater. 4, 113 (1993).
15. M. Ma , "Large scale PVD hard coating process for tribological applications" in Proceeding of 46th Annual Society of Vacuum Coaters Conference, (2003), p. 535.
16. "Ultra-High Temperature Ceramics: Materials for Extreme Environment Applications", edited by W.G. Fahrenholtz, E.J. Wuchina, W.E. Lee, and Y. Zhou (Wiley, Hoboken, NJ, 2014).
17. N. Nedfors, A. Mockute, J. Palisaitis, P.O.Å. Persson, L.-Å. Näslund, and J. Rosén, Surf. Coat. Technol. 304, 203 (2016).
18. T.F. Zhang, B. Gan, S. Park, Q.M. Wang, and K.H. Kim, Surf. Coat. Technol. 253, 115 (2014).

19. F. Kunc, J. Musil, P.H. Mayrhofer, and C. Mitterer, Surf. Coat. Technol. 174, 744 (2003).
20. P.H. Mayrhofer, C. Mitterer, J.G. Wen, J.E. Greene, and I. Petrov, Appl. Phys. Lett. 86, 131909 (2005).
21. A. Mockute, J. Palisaitis, B. Alling, P. Berastegui, E. Broitman, L.-Å. Näslund, N. Nedfors, J. Lu, J. Jensen, L. Hultman, J. Patscheider, U. Jansson, P.O.Å. Persson, and J. Rosén, Scripta Mater. 127, 122 (2017).
22. J. Neidhardt, S. Mráz, J.M. Schneider, E. Strub, W. Bohne, B. Liedke, W. Möller, and C. Mitterer, J. Appl. Phys. 104, 063304 (2008).
23. I. Petrov, A. Hall, A.B. Mei, N. Nedfors, I. Zhirkov, J. Rosén, A. Reed, B. Howe, G. Greczynski, J. Birch, L. Hultman, and J.E. Greene, J. Vac. Sci. Technol. A 35, 050601 (2017).
24. V. Kouznetsov, K. Macak, J.M. Schneider, U. Helmersson, and I. Petrov, Surf. Coat. Technol. 122, 290 (1999).
25. J.T. Gudmundsson, N. Brenning, D. Lundin, and U. Helmersson, J. Vac. Sci. Technol. A 30, 030801 (2012).
26. G. Greczynski, I. Zhirkov, I. Petrov, J.E. Greene, and J. Rosén, J. Vac. Sci. Technol. A 35, 060601 (2017).
27. G. Greczynski, J. Lu, M.P. Johansson, J. Jensen, I. Petrov, J.E. Greene, and L. Hultman, Surf. Coat. Technol. 206, 4202 (2012).
28. G. Greczynski, I. Petrov, J.E. Greene, and L. Hultman, J. Vac. Sci. Technol. A 05E101, 33 (2015).
29. G. Greczynski, and L. Hultman, Vacuum 84, 1159 (2010).
30. J. Bohlmark, M. Lattemann, J.T. Gudmundsson, A.P. Ehiasarian, Y.A. Gonzalvo, N. Brenning, and U. Helmersson, Thin Solid Films 515, 1522 (2006).

31. A. Agarwal and J. H. Lang, Foundations of Analog and Digital Electronic Circuits, 1st ed. (Morgan Kaufman Publishers, San Francisco, United States of America, 2005), chapter 12.2.1.

32. "Atomic, molecular, and optical physics; ionization potentials of atoms and atomic ions," in CRC Handbook of Chemistry and Physics, 84th ed., edited by D. R. Lide (CRC, Boca Raton, FL, 2003), Sect. 10.

33. M.A. Lennon, K.L. Bell, H.B. Gilbody, J.G. Hughes, A.E. Kingston, M.J. Murray, and F.J. Smith, J. Phys. Chem. Ref. data 17, 1285 (1988).

34. As the peak target power is increased, sputtered-ejected B and Ti ions are returned to the target at different rates due to differences in plasma ionization probabilities. This changes the effective sputtering yields of B and Ti; the Ti sputtering yield decreases and, as a consequence, the Ti coverage at the target surface is increased (the B coverage decreases) until the steady-state composition of the sputtered flux again equals that of the bulk target.

35. A. Anders, J. Appl. Phys. 121, 171101 (2017).

36. D. Horwat, and A. Anders, J. Appl. Phys. 108, 123306 (2010).

37. J. Alami, K. Sarakinos, G. Mark, and M. Wuttig, Appl. Phys. Lett. 89, 154104 (2006).

38. M. Desecures, L. de Poucques, T. Easwarakhanthan, and J. Bougdira, Appl. Phys. Lett. 105, 181120 (2014).

39. S. Loquai, O. Zabeida, J. E. Klemberg-Sapieha, and L. Martinu, Appl. Phys. Lett. 109, 114101 (2016).

40. P. Raman, J. Weberski, M. Cheng, I. Shchelkanov, and D. N. Ruzic, J. Appl. Phys. 120, 163301 (2016).

41. W.D. Sproul, D.J. Christie, and D.C. Carter, "The reactive sputter deposition of aluminum oxide coatings using high power pulsed magnetron sputtering (HPPMS)", in Proceeding of 47th Annual Society of Vacuum Coaters Conference, (2004), p. 96.

42. D.J. Christie, J. Vac. Sci. Technol. A 23, 330 (2005).

43. J. Vicek, and K. Burcalová, Plasma Sources Sci. Technol. 19, 065010 (2010).

44. P. Sigmund, J. Vac. Sci. Technol. A 17, 396 (1980).

45. M. W. Thompson, Phys. Rep. 69, 335 (1981).

46. Y. Yang, K. Tanaka, J. Liu, and A. Anders, Appl. Phys. Lett. 106, 124102 (2015).

47. A. Anders, M. Panjan, R. Franz, J. Andersson, and P. Ni, Appl. Phys. Lett. 103, 144103 (2013).

48. M. Samuelsson, J. Jensen, U. Helmersson, L. Hultman, and H. Högberg, Thin Solid Films 526, 163 (2012).

49. Truncating the current pulse at the maximum amplitude, rather than allowing for a slow decay, while sputtering a Ti target in HiPIMS mode at a peak target current density of 1 A/cm^2 in 3 mTorr of Ar, resulted in a dramatic drop in the intensity of Ar^+ ions incident at the substrate plane (reference 50).

50. G. Greczynski, I. Zhirkov, I. Petrov, J. E. Greene, and J. Rosen, Thin Solid Films 642, 36 (2017).

51. S. M. Rossnagel, J. Vac. Sci. Technol. A 6, 19 (1988).

52. D.W Hoffman, J. Vac. Sci. Technol. A 3, 561 (1985).

53. S. Schiller, K. Goedicke, J. Reschke, V. Kirchhoff, S. Schneider and F. Milde, Surf. Coat. Technol. 61, 331 (1993).

54. W.D. Sproul, D.J. Christie, and D.C. Carter, Thin Solid Films 491, 1 (2005).

55. J.E Greene, J. Vac. Sci. Technol. A 35, 05C204 (2017), Section IV.J.4.

Table 1. Electron-impact ionization cross-sections $\sigma(E_e)$ for Ti, B, and Ar as a function of electron energy E_e.[35]

	$\sigma(E_e)$ [$\times 10^{-16}$ cm^2]			
	E_e = 10 eV	E_e = 25 eV	E_e = 50 eV	E_e = 100 eV
Ti^+	5.93	7.46	5.52	3.63
B^+	0.11	2.15	2.46	2.04
Ar^+	--	2.12	2.93	2.49

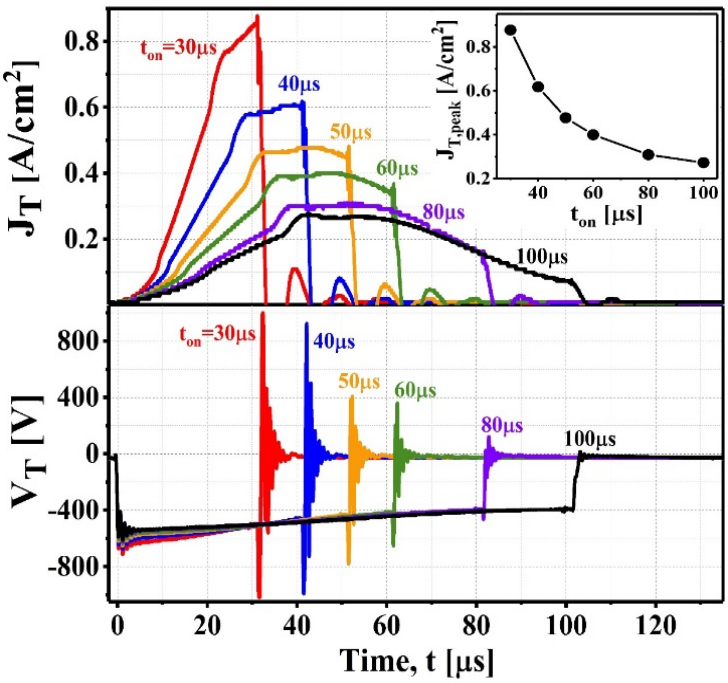

Fig. 1. Target current density J_T and voltage V_T waveforms recorded during HiPIMS sputtering of TiB_2 in Ar at 3 mTorr as a function of the pulse length t_{on}. The target power is 3 kW with a 1 kHz pulse frequency.

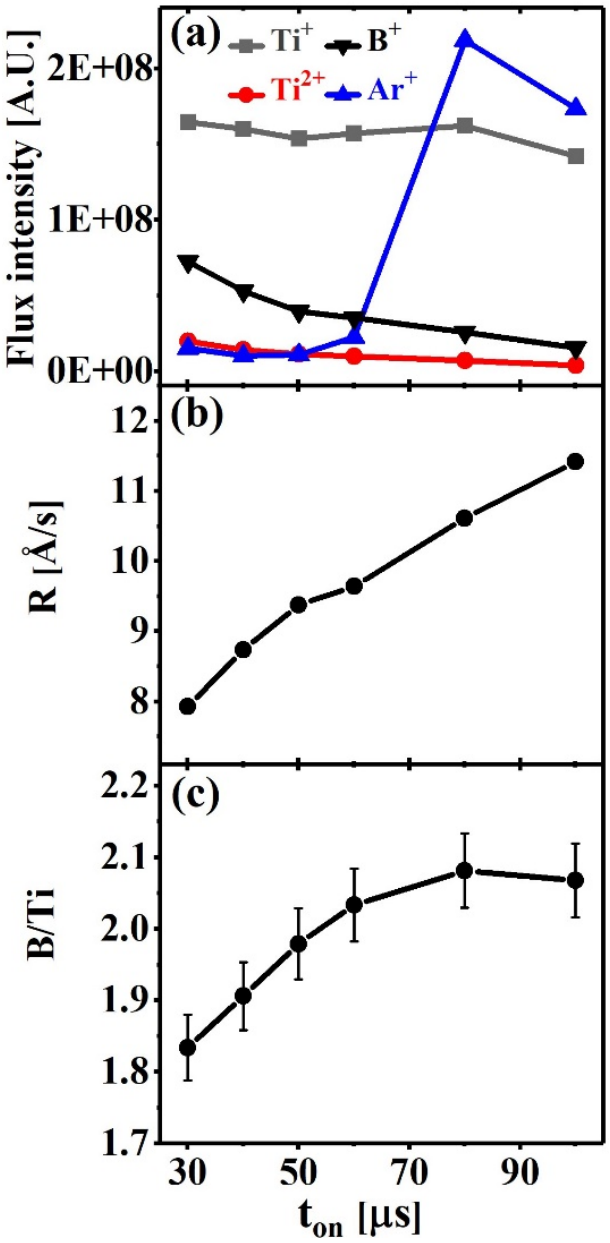

Fig. 2. (a) Elemental ion intensities F_i (i = Ti^+, Ti^{2+}, B^+, Ar^+) incident at the substrate plane, (b) TiB_x film growth rate R, and (c) B/Ti film composition as a function of the pulse length ton during HiPIMS sputtering of a TiB_2 target in Ar at 3 mTorr. The target power is 3 kW with a 1 kHz pulse frequency.

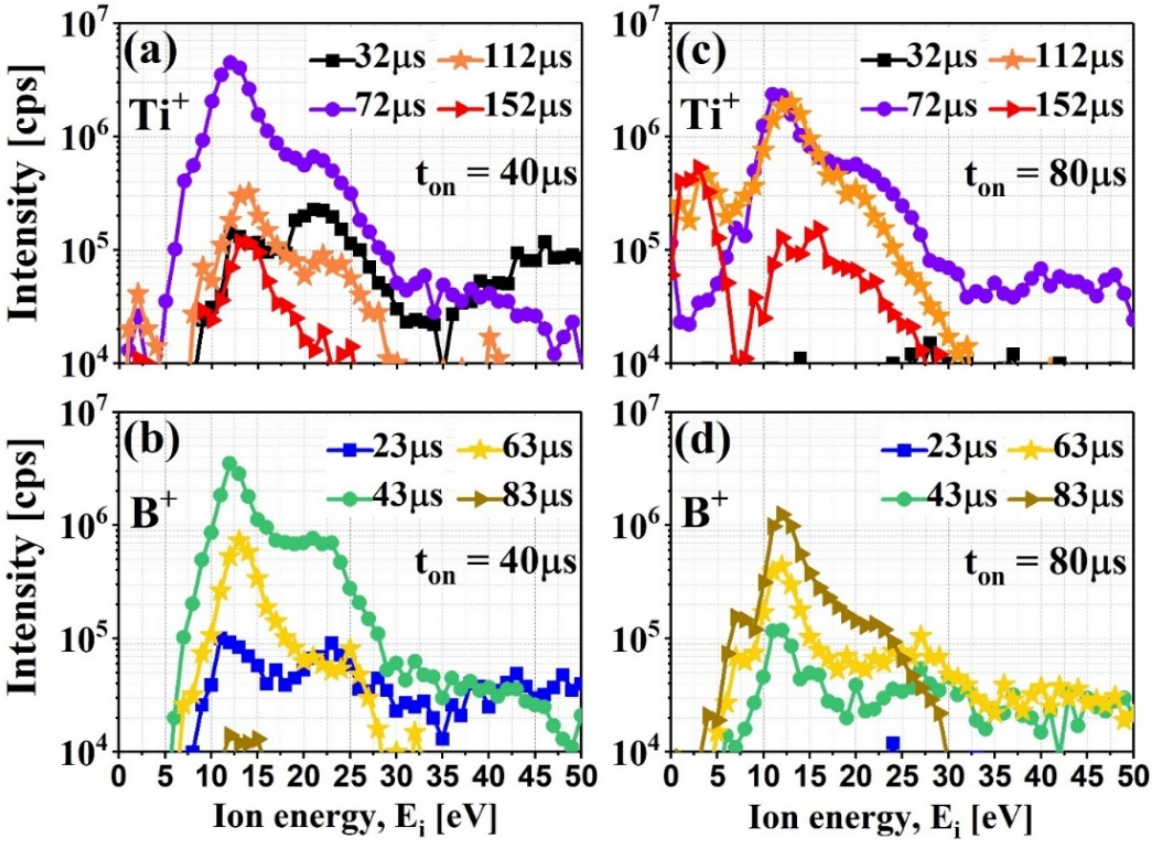

Fig. 3. Ti^+ and B^+ IEDFs acquired with (a) and (b) t_{on} = 40 μs, and (c) and (d) 80 μs pulse lengths, during HiPIMS sputtering of a TiB_2 target in Ar at 3 mTorr. The target power is 3 kW with a 1 kHz pulse frequency. Times indicated in the legends correspond to the number of μs from the onset of the HiPIMS pulse at which the IEDF was acquired.